Green infrastructure for coastal flood protection: The longitudinal impacts of green infrastructure patterns on flood damage

Wonmin SOHN [a,*], Jinhyun BAE [b], and Galen NEWMAN [b]

[a] *School of Planning, Design & Construction, Michigan State University, United States*

[b] *Department of Landscape Architecture and Urban Planning, Texas A&M University, United States*

* Corresponding author at: School of Planning, Design & Construction, Michigan State University, 552 West Circle Drive, Room 201C, East Lansing, MI 48824, USA; Tel: +1-517-353-0677

E-mail addresses: wonmin@msu.edu (W. Sohn), jinhyun2009@tamu.edu (J. Bae), gnewman@arch.tamu.edu (G. Newman)

Declarations of interest: none.

1. Introduction

Flooding causes devastating structural damage both nationally and globally. Between 1980 and 2019, flood-inducing storm events and hurricanes led to $1,340 billion in damage in the United States (US), accounting for 76% of total losses for all billion-dollar climate events during that period [1]. Driven by climate change, the total damage cost of floods has increased over time, breaking the record for the greatest damage in the last five years (2015 to 2019). In coastal areas, storm surges and excessive land transformation are the major drivers of rising flood damage [2-4]. Texas and Florida, particularly, have experienced the most substantial losses [5]. The growing population and expanding impervious surfaces have limited the capacity of natural ecosystems to capture and store rainwater, increasing flood vulnerability [6]. After examining 34 major hurricanes in the US that occurred since 1980, Costanza et al. [7] argued that on average, a loss of 1 ha of coastal wetland led to $33,000 of flood damage from a hurricane event. Brody et al. [8] also reported that a 1-acre loss of naturally occurring wetlands along the Gulf coast increased insured property loss by $1.5 million per year. The lower 48 US states, however, lost 110 million acres of wetlands between 1600 and 2009 [9]. The US Army Corps of Engineers has invested an average $2 billion into constructing flood control structures every year since the 1940s to attenuate flooding risks accelerated by land conversion, but this effort is still not sufficient to compensate for the losses we face today [10]. As the frequency of flood risk increases, the need for ecological planning and design strategies for enhancing flood protection grows. Given this context, green infrastructure (GI) has gained attention as a promising planning tool.

The origins of GI are rooted in urban planning and conservation theory. This concept evolved from ecological planning and eventually was integrated into low impact development

(LID), originally an engineered-based solution to control stormwater runoff near pollutant sources which sought to also preserve hydrologic patterns of pre-development [11, 12]. While LID techniques focus on the hydrologic protection of construction sites or small watersheds, the notion of GI embraces the far-reaching benefits of multi-scale green spaces as interactive systems, emphasizing the manifold ecosystem services that can be offered to humans. Scientifically, GI is often defined as "an interconnected network of green space that conserves natural ecosystem values and provides associated benefits to [the] human population" (Benedict & McMahon, 2012, p. 12). After the Conservation Fund and US Department of Agriculture Forest Service formed government and non-government working groups in 1999, GI became an integral part of local, regional, and state plans and policies. As a way of promoting human health and biodiversity, GI establishes green space networks and links ecologically functional habitats, enhancing species richness and productivity [14, 15]. It also provides cooling effects to heated urban areas by modifying airflow and heat flux [16]; simultaneously, GI also serves as an important surface water supply source by intercepting and storing rainwater during wet seasons [17]. In addition, as is also the case with LID, GI contributes to hazard mitigation by retaining stormwater, reducing pollutant concentrations, and increasing the lag time between rainfall and runoff, thus helping moderate losses from flooding [12, 18, 19].

Traditionally, flood mitigation approaches have been based on both structural and non-structural mechanisms [20, 21]. Structural mitigation is a technical approach that considers engineering safety features such as dams, dikes, reservoirs, and water channels to moderate the impacts of development in hazard-prone areas [22]. Non-structural measures are based on land-use planning, policies, and education designed to protect environmentally sensitive areas [23]. With both structural and non-structural approaches, effective implementation and maintenance of

GI can be achieved. Previous studies have documented how these efforts have led to successful flood control on national, regional, and local scales [24-27]. For example, Brody and Highfield [26] explored 450 communities participating in the Community Rating System developed by the Federal Emergency Management Agency (FEMA), finding that from 1999 to 2009, communities with more credits for open space preservation had less flood damage. A survey also revealed that respondents were willing to pay an average of $6.4 more per year to adopt conservation easement policies that protected river buffers from floods [25]. However, these studies focused on preserving the quantity of GI, leaving unaddressed the influence of GI quality on flooding.

Recently, a few studies have conducted cross-sectional analyses to examine the spatial configurations of GI. They found that larger areas of GI with irregular patch shapes helped to minimize stormwater runoff [28-31]. Kim and Park [32] assessed 108 watersheds in the four largest Texas metropolitan statistical areas, concluding that less fragmented patterns of GI were important to mitigating peak runoff. Similarly, Brody et al. [18] argued that large and continuous natural open spaces contributed to reducing flood losses along the Gulf of Mexico in the US. Studies examining GI connectivity have shown inconsistent results; on a watershed level, an increase in connectivity was found to lead either to an increase or decrease in peak runoff in urban and suburban watersheds [32]. Another study reported that, on a city scale, connectivity was negatively associated with runoff [31]. This inconsistency demonstrates the need for additional empirical studies to confirm the impact of GI patterns on flood mitigation at diverse scales [33].

Prior studies lack longitudinal assessments of GI patterns. As a consequence, the temporal changes in GI configurations that most affect long-term flooding have rarely been investigated. In particular, coastal regions have suffered from escalations in flood risk over time due to increased demands for urbanization and growing frequencies in high-intensity tropical cyclones [34, 35]. Given this environmental challenge, routine monitoring of GI provides insights into how to maintain key landscape forms in the long term, in order to reduce devastating losses from floods and enhance coastal resilience. To address these challenges, this study longitudinally assessed the monetary benefits of implementing and preserving quality GI patterns by exploring flood damage costs reported along the Gulf of Mexico in Texas from 2000 to 2017. This research will specifically answer a question of how temporal and geographic variations in size, shape, isolation, fragmentation, and connectivity of GI patches affect county-level flood loss.

2. Methods

2.1. Study area

The study area in this research includes 36 Texas coastal watershed counties along the US Gulf of Mexico (see Figure 1). According to the National Oceanic and Atmospheric Administration [36], a coastal watershed county is defined as one in which: 1) at least 15% of the total county area resides within a coastal watershed, or 2) the county partially includes at least 15% of an eight-digit hydrologic unit code (HUC) watershed defined by the US Geological Survey (USGS). The coastal counties selected in this study were subject to repeated flood damage from tropical hurricanes during the Atlantic hurricane season, more so than any other state in the United States [37]. Surface flow across these counties drains into the Gulf of Mexico, implying that changes in land use and GI configuration in the study area would directly affect downstream flooding. The flood damage within the study area spatially and temporally varied across these counties, serving as an important criterion for site selection. Out of 41 coastal watershed counties located in Texas, we excluded those in which the population was less than 10,000; these were likely to lack the resources to initiate planning efforts to improve GI, limiting the policy application of this research [38].

The increasing flooding potential of the study area is attributable to the environmental condition. The area is dominantly characterized by flat terrain, clayey and loamy soil of low to moderate soil permeability, and low-lying land [39]. Increasing amounts of impervious surfaces and population growth at the expense of wetlands in this region have imposed human-dominated stresses on regional water resources, causing the depletion of water bodies and land subsidence in certain areas [40, 41]. By the late 20th Century, coastal Texas had already lost 210,600 acres of wetlands (5,700 acres per year on average), yet the Gulf of Mexico region had experienced over a 150% population increase since 1960 [42, 43]. The coastline counties are even vulnerable to storm surges during hurricane events, and the projected increase in sea level driven by climate change will exacerbate future flooding risk (e.g., a 4.4-5.5 ft rise is forecasted by 2100) [44]. Given these environmental challenges, the total flood damage reported in the study area was over $80 billion from 1990 to 2017 [45]. Major devastating events include Tropical Storm Imelda in 2019, Category 4 Hurricane Harvey in 2017, Category 4 Hurricane Ike in 2008, Category 5 Hurricane Rita in 2005, Tropical Storm Allison in 2001, and others [46].

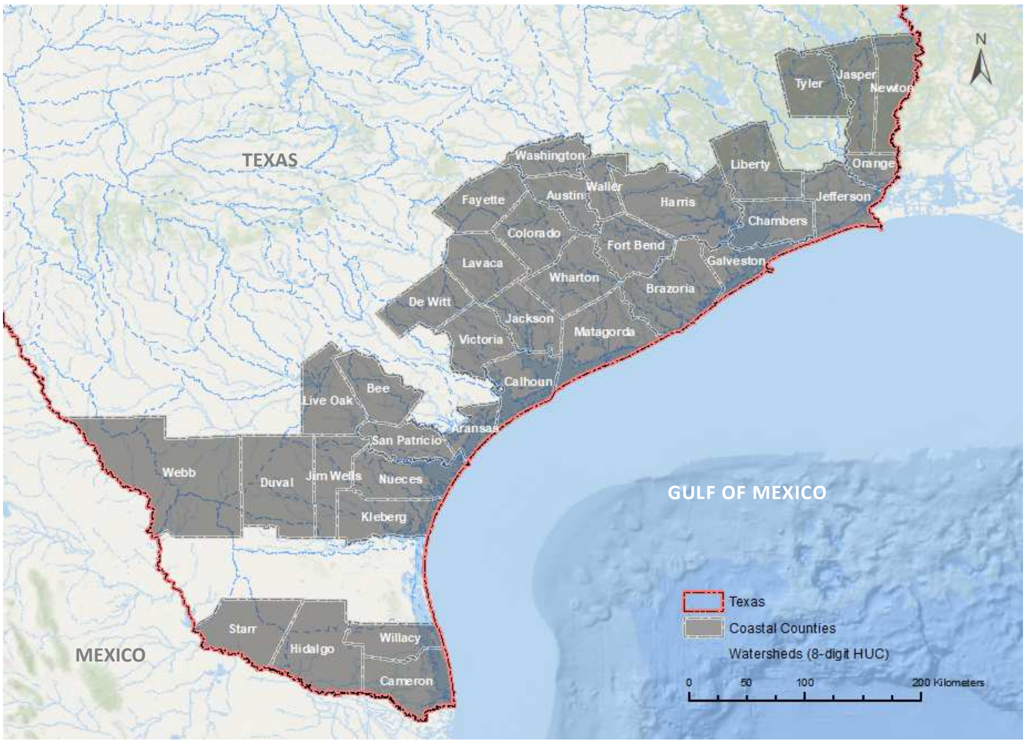

Figure 1. The selected coastal watershed counties in Texas.

2.2. Variables measurement

2.2.1. Flood loss

Property damage per capita, as obtained from the Spatial Hazard Events and Losses Database (SHELDUS), represents the US dollar value of direct property losses (adjusted for inflation to 2015 dollars) divided by the annual county population (see Table 1). Out of 18 types of natural hazards reported by SHELDUS, this study focused only on flood events in coastal regions that mainly were caused by heavy or extreme storm events and storm surges. For the longitudinal assessment, we computed the total damage cost per capita as a dependent variable for four time-windows at a consistent interval (i.e., 2000 to 2002, 2005 to 2007, 2010 to 2012, and 2015 to 2017). The values were log transformed in the model specifications to approximate normality.

The National Weather Service is responsible for approximating and reporting federal estimates of flood losses in the National Climatic Data Center's Storm Data, which serve as the source of SHELDUS. It is important to note that these monetary estimates can be positively or negatively biased during the conversion of ordinal to numeric values and when data are merged from multiple sources [47]. Although caution is required for their use, several studies has supported the reliability of SHELDUS data [37, 48, 49].

Table 1. Variable measurement

Variable	Measurement (unit)	Source	Range	Mean (SD)
Dependent variable				
Flood damage cost	Logged total 3-year property damage per capita	SHELDUS	-13.82–11.24	0.07 (7.18)
	Total 3-year property damage per capita (US$)	SHELDUS	0–76,269.52	3,186.76 (9,676.87)
Independent variables				
Spatial patterns of GI				
PLAND	Percentage of GI (%)	USGS NLCD	16.20–95.13	48.35 (21.10)
SHAPE	Mean shape index (none) $\sum_{i=1}^{n} \frac{.25\, p_i}{\sqrt{a_i}} \Big/ n$	USGS NLCD	1.21–1.96	1.54 (0.18)
PROX	Mean proximity index (none) $\sum_{s=1}^{n} \frac{a_{is}}{h_{is}^2} \Big/ n$	USGS NLCD	622.00–903,398.70	100,719.40 (175,505.60)
ENN	Mean nearest neighbor distance (m) $\sum_{i=1}^{n} h_i \Big/ n$	USGS NLCD	70.26–99.77	84.29 (5.38)
COHESION	Patch cohesion index (none) $\left[1 - \frac{\sum_{i=1}^{n} p_i}{\sum_{i=1}^{n} p_i \cdot \sqrt{a_i}}\right] \cdot \left[1 - \frac{1}{\sqrt{Z}}\right] \cdot (100)$	USGS NLCD	98.09–99.99	99.65 (0.40)
GYRATE	Area-weighted mean radius of gyration (km) $\sum_{i=1}^{n}\left[\left(\sum_{r=1}^{z}\frac{h_{ir}}{z}\right)\left(\frac{a_i}{\sum_{i=1}^{n} a_i}\right)\right]$	USGS NLCD	1.69–38.68	12.05 (8.14)
Control variables				
Socioeconomic attributes				
Housing value density	Housing value density assessed per unit area ($/m^2)	USCB	0.02–40.68	2.21 (5.44)
Undereducation	Percentage of persons with no high school diploma (%)	USCB	10.81–65.30	25.91 (9.74)
Race	Percentage of non-Hispanic whites (%)	USCB	0.76–85.90	48.42 (24.00)
Built environment				
Impervious area	Percentage of impervious area (%)	USGS NLCD	0.31–31.02	2.70 (4.88)
Dams	Total number of dams	USACE	0–108	17.99 (20.38)
Climatic and geophysical environment				
Precipitation	Mean annual precipitation (mm)	PRISM	451.90–2,222.02	1,087.92 (406.28)
Duration of flood events	Mean annual duration of flood events (days)	SHELDUS	0–30.70	2.89 (4.05)

Surface elevation	Mean surface elevation (km)	USGS NHD Plus	0.003–0.18	0.05 (0.04)
Floodplain area	Percentage of 100-year floodplain area (%)	FEMA	8.76–59.05	27.08 (14.02)
Slope	Mean slope (%)	USGS NHD Plus	0.25–3.48	1.22 (1.03)
Soil permeability	Mean saturated hydraulic conductivity (μm/s)	NRCS SSURGO	1.23–34.08	9.79 (6.58)
Adjacency to coast	Counties bordering the Gulf of Mexico (0/1)	TxDOT	0/1	0.44 (0.50)
Distance to coastline	Nearest Euclidean distance to the Gulf of Mexico coastline from the county centroid (km)	TxDOT	0.12–158.37	56.44 (43.01)

Note. n = number of patches of the selected patch type (class); a_i = area (m^2) of the patch i; a_{is} = area (m^2) of the patch is within the 400m search radius of patch i (i.e., the search buffer created from the centers of the edge cells of the focal patch); p_i = perimeter of the patch i; h_i = distance (m) from patch i to the nearest neighboring patch of the same type, based on edge-to-edge distance; h_{is} = distance (m) between patch is and patch is, based on edge-to-edge distance computed from cell center to cell center; h_{ir} = distance (km) between cell ir placed in patch i and the centroid of patch i based on the cell's center-to-center distance; Z = total number of cells in the landscape; z = number of cells in patch i.

SHELDUS = Spatial Hazard Events and Losses Database for the United States; USGS NLCD = United States Geological Survey's National Land Cover Database; USCB = United States Census Bureau; USACE = United States Army Corps of Engineers; USGS NHD = United States Geological Survey's National Hydrography Dataset; NRCS SSURGO = Natural Resources Conservation Service's Soil Survey Geographic Database; TxDOT = Texas Department of Transportation; PRISM = Parameter-elevation Regressions on Independent Slopes Model.

2.2.2. Spatial patterns of green infrastructure

The independent variables in this study included a series of GI configuration indicators derived from the 30-meter resolution landcover maps for 2001, 2006, 2011, and 2016, produced by the USGS (overall accuracy = 90%, 89%, 88%, and 88%, respectively) (Yang et al., 2018). We reclassified the Level II system developed by Anderson into a single GI class, combining open space (21), deciduous forest (41), evergreen forest (42), mixed forest (43), shrub/scrub (52), grassland/herbaceous (71), woody wetlands (90), and emergent herbaceous wetlands (95).

Based on previous studies [2, 28, 29, 31, 32, 51], potential indicators of GI configuration for local flooding were computed for each county using FRAGSTATS version 4.2.1. These indicators included percentage of landscape (PLAND), mean shape index (SHAPE), mean proximity index (PROX), mean nearest neighbor distance (ENN), patch cohesion index (COHESION), and area-weighted mean radius of gyration (GYRATE); together, these describe the size, shape, isolation/fragmentation, and connectivity of the GI patches (see Table 1). PLAND quantifies the total area of GI as a percentage. SHAPE is a measure of the mean shape complexity, with larger values implying the GI patches are of a more irregular shape. PROX and ENN collectively measure the levels of isolation and fragmentation, respectively, with higher values indicating larger GI patches in closer proximity and with longer edge-to-edge distances between them. Finally, COHESION and GYRATE jointly compute physical connectivity; values increase if the GI patches are more clumped and connected [52].

2.2.3. Socioeconomic attributes

Socioeconomic variables such as income or wealth, education, and race/ethnicity have been shown to serve as drivers of disproportionate flooding impacts [53]. Previous studies have argued that people with less economic cabbies, lower levels of knowledge, and a minority status are more vulnerable to flood damage, due to their limited protective measures and means of preparation [54-58]. To control for these socioeconomic impacts, we measured housing value density, income, education level, and race as control variables (see Table 1). Income was dropped from the final models to avoid multicollinearity problems.

We retrieved all socioeconomic data from the US Census Bureau's 2000 and 2010 decennial census as well as the the American Community Survey five-year estimates; these data were then aggregated by county. Similar to previous studies, we linearly interpolated the 2006 value data from the decennial census [59, 60]. The housing value assessed per unit area (i.e., the estimate of what the property would sell for if it were for sale) was calculated as a proxy indicator of wealth and log transformed in the final models to normalize its distribution [61, 62].

In the model specifications, education level and race denoted the percentage of persons with no high school diploma and non-Hispanic whites, respectively (see Table 1).

2.2.4. Built environment

As a major built environment factor, impervious surfaces contribute to increasing flooding risks in urbanized areas. They limit the capacity of land to store rainwater and promote the rapid discharge of runoff through underground sewer systems, thus increasing both flood volume and peak flow [11, 63, 64]. To mitigate this adverse impact, dams are engineered structures constructed to regulate flood volume by forming reservoirs [6]. However, when rainfall exceeds the design capacity of a reservoir, an uncontrolled stormwater release from a dam can result in devastating downstream flooding, as was seen with the Addicks and Barker reservoirs in Houston, Texas during Hurricane Harvey [65]. To control for the effects of these built environment variables, we used the USGS's 30-meter resolution imperviousness data produced in 2001, 2006, 2011, and 2016 to compute the percentage of impervious surface for each county (see Table 1). For the same periods, the number of dams was also counted, using geographic data obtained from the US Army Corps of Engineers.

2.2.5. Climatic and geophysical environment

Climatic factors such as storm size and duration decisively affect flood magnitude. Larger storm amounts over longer durations accelerate soil saturation, forming surface water seals and increasing waterlog hazards [12]. Geophysical features such as surface elevation, flood plain area, slope, soil permeability, and proximity to the coast also play critical roles in escalating flood potential. Low-lying areas such as floodplains are more prone to flooding, due to the shallow groundwater depth [6, 66]. While a sloping terrain speeds up surface flow, a flat topography can dissipate the flow's momentum, causing poor drainage [67]. Similarly, low-permeability soil degrades the infiltration capacity, increasing the chance of water ponding. During major rainfall events, storm surges add another flood burden to areas situated along coastlines [68, 69].

To quantify these contributing factors, mean annual precipitation during the reported flood damage periods was collected from the Parameter-elevation Regressions on Independent Slopes Model (PRISM) Climate Group dataset. Corresponding mean annual durations of flood events were also computed using SHELDUS. Unlike these climatic factors, we assumed that geophysical variables barely changed over time, inputting them as time-invariant variables into our models. Mean surface elevation and slope were computed based on the 30-meter digital elevation models obtained from the USGS. We mapped the 100-year floodplain based on the Q3 Flood Data and National Flood Hazard Layer provided by FEMA. The saturated hydraulic conductivity acquired from the Soil Survey Geographic Database (SSURGO) maintained by the Natural Resources Conservation Service was quantified to represent soil permeability. Finally, using the jurisdictional boundaries retrieved from the Texas Department of Transportation (TxDOT), we measured the nearest Euclidean distance from the county centroid to the Gulf of Mexico coastline, as well as the binary value of whether the county bordered the coast.

2.3. Data analysis

Unlike single cross-sectional or time-series data, a panel dataset consists of both cross-sectional and time-series dimensions, denoted as $i = 1, \ldots, N$ and $t = 1, \ldots, T$, respectively. To account for the individual and temporal heterogeneity of the dataset collected in this study, we employed a spatial panel data model, an advanced tool developed to capture the complexity of cross-sectional time-series behaviors and phenomena that are spatially correlated, as compared to using two traditional, non-spatially weighted models [70].

Traditionally, three techniques can be applied in standard panel data modeling: pooled ordinary least squares (OLS), fixed effects, and random effects. The pooled OLS method disregards the panel structure of data and produces the most restrictive model. As a baseline model, we developed the pooled OLS model for *NT* observations, as follows:

$$F = \beta_0 + GI\beta_1 + S\beta_2 + B\beta_3 + C\beta_4 + G\beta_5 + \varepsilon, \qquad \text{Eq. 1}$$

where F is an $(NT \times 1)$ vector of logged flood losses; GI is an $(NT \times i)$ matrix of the GI's spatial pattern variables; S is an $(NT \times j)$ matrix of the socioeconomic variables; B is an $(NT \times k)$ matrix of the built environment variables; C is an $(NT \times l)$ matrix of the climatic variables; G is an $(NT \times m)$ matrix of the geophysical variables; β_0 is an $(NT \times 1)$ vector of the constant; β_1, β_2, β_3, β_4, and β_5 are $(i \times 1)$, $(j \times 1)$, $(k \times 1)$, $(l \times 1)$, and $(m \times 1)$ vectors of estimated parameters, respectively; and ε is an $(NT \times 1)$ vector of idiosyncratic error terms with a constant variance.

Unlike pooled OLS models, fixed and random effects models take the panel structure of a dataset into account based upon correlations between explanatory variables and the unobserved effects of entities (in this case, counties). The advantage of using a fixed effects method is that the researcher can control for the unobserved effects of time-invariant variables, whether or not they are measured [71, 72]. Conversely, random effects models allow for the investigation of specified time-invariant causes of dependent variables (such as certain geophysical attributes in the present study). Hausman [73]Based on the results of the Hausman specification test [73], a two-way fixed effects model was selected over a random effects model for the panel data in this study. Considering that counties not being randomly sampled from a population and fixed effects estimation is generally better at supporting policy analysis [74], the fixed effects estimator was determined to be optimal for this study.

Using the balanced panel data, we stacked the observations as successive cross-sections for $t = 1, \ldots, T$. In the stacked form, the two-way fixed effects model could then be formulated as follows:

$$F_t = \beta_0 + GI_t\beta_1 + S_t\beta_2 + B_t\beta_3 + C_t\beta_4 + \mu + \lambda_t\iota_N + \varepsilon_t, \qquad \textit{Eq. 2}$$

where F_t is an $(N \times 1)$ vector of logged flood losses; GI_t is an $(N \times i)$ matrix of the GI's spatial pattern variables; S_t is an $(N \times j)$ matrix of the socioeconomic variables; B_t is an $(N \times k)$ matrix of the built environment variables; C_t is an $(N \times l)$ matrix of the climatic variables; μ is an $(N \times 1)$ vector of the unobserved county-specific effects determined by time invariant variables not included in this model; λ_t is a scalar time-specific effect; ι_N is an $(N \times 1)$ vector of ones; and ε_t is an $(N \times 1)$ vector of idiosyncratic error terms with a constant variance for time period t.

However, this standard method can still sometimes lead to misinterpretations, if the sample observations are spatially or temporally correlated. The global Moran's I statistics for each time period implied that significant spatial or cross-sectional dependence was particularly present in the dependent variable of flood damage. To control for this autocorrelation effect, we developed and tested the performance of diverse, advanced spatial panel data models (i.e., the mixed regressive spatial autoregressive (SAR) model, spatial error model (SEM), spatial Durbin model (SDM), and spatial autoregressive combined (SAC) model) [75, 76]. The Lagrange multiplier test, a diagnostic test that detects errors resulting from the omission of spatial autoregressive parameters [77, 78], and a subsequent model interpretation revealed that the SEM would be a better fit with theoretically consistent signs. While the SAR and SDM presume the presence of spatial dependence in independent or dependent variables, the SEM includes spatially correlated errors in the model, in this case assuming that the flood loss error of an observation would affect that of a neighbor. The SEM with spatial fixed effects was specified as follows:

$$F_t = \beta_0 + GI_t\beta_1 + S_t\beta_2 + B_t\beta_3 + C_t\beta_4 + \mu + \lambda_t\iota_N + \varepsilon_t, \qquad \textit{Eq. 3}$$

$$\varepsilon_t = \theta W_N \varepsilon_t + u_t = (I_N - \theta W_N)^{-1} u_t$$

where θ is a spatial autoregressive parameter; W_N is an ($N \times N$) weight matrix for the cross-sectional dimension, in which each component $w_{ij} \in W_N$ denotes the spatial weight of associations between neighbor units *i* and *j*; I_N is an ($N \times N$) identity matrix; and u_t is an ($N \times 1$) vector of idiosyncratic errors independently distributed across cross-sections, with a constant variance for time period *t*. We produced the weight matrix W_N using the Queen's contiguity method, based on the assumption that neighboring counties would affect the flood losses of a target county. Consequently, the weight of bordering counties was assigned a 1, and 0 was assigned to the others [78]. The final weight matrix was row-standardized to have the sum of elements in each row be 1. In spatial panel modelling, it is important to note that this weight remains constant over time. If error terms are heteroskedastic, one-way clustered standard errors must also be computed [79, 80].

3. Results

3.1. Spatial and temporal variations in flood losses

During the study period, the selected coastal watershed counties experienced 731 flood events, resulting in a total of approximately $78 billion in accumulated damage costs. The most damaged counties were clustered in north-eastern Texas along the Gulf of Mexico (see Figure 2). The top three counties were Aransas County ($76,346 per person), Galveston County ($61,661 per person), and Newton County ($41,231 per person), while the bottom three were Duval County ($4.90 per person), Live Oak County ($17.20 per person), and Kleberg County ($21.70 per person). Regarding the flood frequency, Harris County, which includes Houston, the largest city in Texas, experienced the highest number of flood events (a total of 98) during the study period, with $4,485 in flood loss per capita. In contrast, only five flood events occurred in Aransas County, but these represented the greatest total flood damage reported in the sample, implying the highest intensity of flood events taking place during the study period.

The mean total flood loss varied substantially by time period, as shown in Table 2. Flood damage across the counties was the lowest between 2010 and 2012 and the highest between 2015 and 2017 ($35.4 and $8,940 per person, respectively). This trajectory corresponded with rainfall trends; the respective terms were the driest and wettest during the entire study period. In particular, the 2011 drought recorded the lowest precipitation in Texas since 1910 [81], while Hurricane Harvey brought historic flooding in 2017 [46].

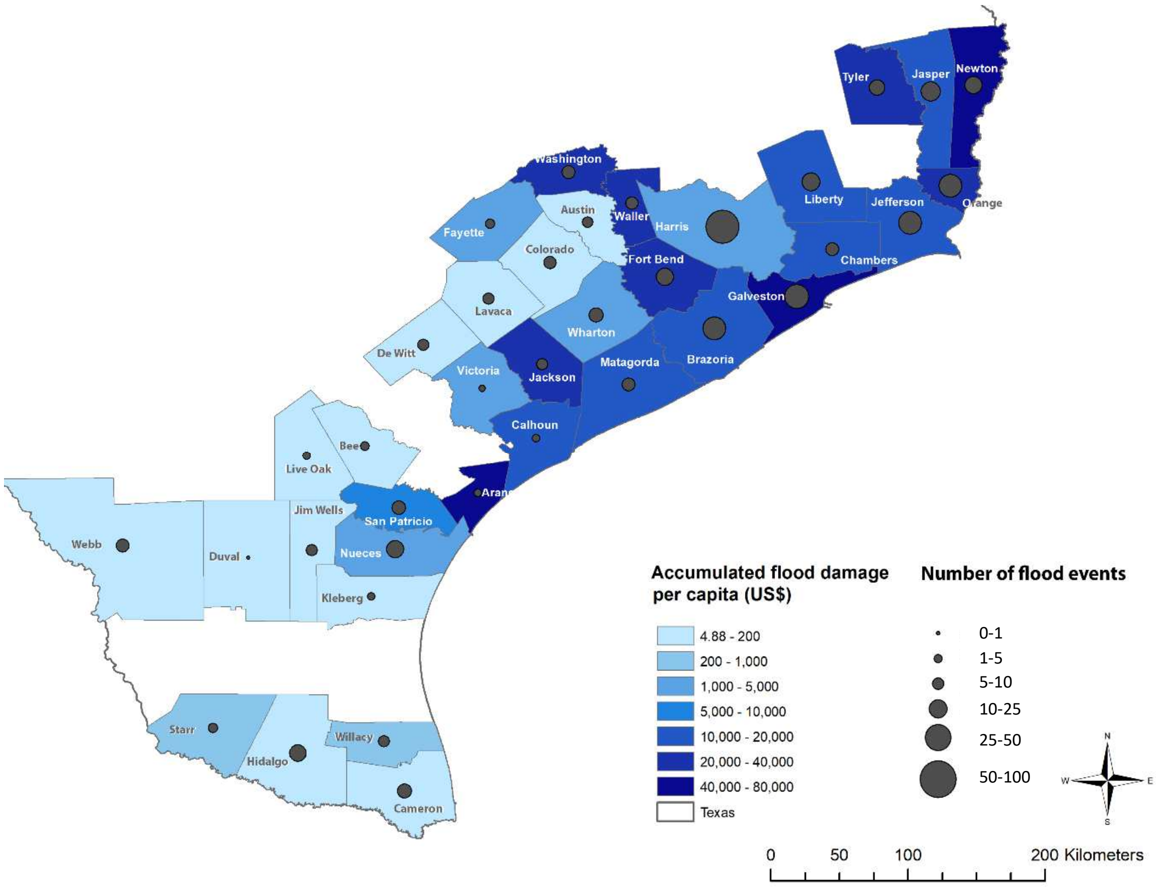

Figure 2. Accumulated flood damage cost per capita in the selected coastal watershed Texas counties during the study period.

Table 2. Mean values of major variables by time period.

Variable	Period 1 (2000-2002)	Period 2 (2005-2007)	Period 3 (2010-2012)	Period 4 (2015-2017)
Dependent variable				
Flood damage per capita (US$)	1,690.80 (4,581.07)	2,080.89 (6,615.64)	35.36 (120.42)	8,940.00 (16,431.86)
Independent variables				
Spatial patterns of GI				
PLAND (%)	49.30 (20.57)	49.06 (20.64)	48.92 (20.64)	46.12 (23.18)
SHAPE	1.57 (0.19)	1.57 (0.19)	1.56 (0.18)	1.44 (0.13)
PROX	106,380.50 (184,069.30)	105,051.40 (177,969.30)	103,768.90 (175,163.50)	87,676.70 (171,392.60)
ENN (m)	83.81 (4.82)	83.75 (4.80)	83.63 (4.72)	85.96 (6.77)
COHESION	99.70 (0.32)	99.69 (0.34)	99.67 (0.38)	99.55 (0.51)
GYRATE (km)	12.29 (8.07)	12.35 (8.19)	12.23 (9.30)	11.34 (8.31)
Control variables				
Socioeconomic attributes				
Housing value density ($/m^2)	1.20 (1.93)	1.92 (4.44)	2.63 (5.93)	3.11 (7.44)
Undereducation (%)	30.87 (10.01)	27.06 (9.06)	24.17 (8.88)	21.53 (8.75)
Race (%)	51.45 (24.59)	49.26 (24.27)	47.31 (23.94)	45.65 (23.75)
Built environment				
Impervious area (%)	2.41 (4.32)	2.61 (4.78)	2.81 (5.13)	2.97 (5.39)
Dams (count)	17.86 (20.51)	17.97 (20.61)	18.06 (20.64)	18.06 (20.64)
Climatic environment				
Precipitation (mm)	1,124.29 (391.18)	1,066.49 (319.67)	816.81 (214.82)	1,344.11 (477.59)

Duration of flood events (days)	3.94 (4.45)	1.58 (2.11)	2.59 (5.58)	3.43 (2.91)
Observations (N)	36	36	36	36

Note. Standard deviations are denoted in parenthesis; geophysical variables are assumed to be time-invariant and thus are not included in this table.

3.2. Temporal variations of factors contributing to flood loss

The descriptive statistics reported in Table 2 demonstrate temporal changes in the GI configuration, socioeconomic status, and built and climatic environments of the selected coastal watershed counties. Overall, the GI gradually degraded from 2000 to 2017. The mean total amount of GI was reduced by 3.2 percent points over the study period. The reduced values for SHAPE, PROX, COHESION, and GYRATE indicate a decreasing complexity in the GI patterns and losses in proximity and physical connectivity between GI patches over time. Increasing ENN values also indicate an escalating isolation of GI patches. It is important to note that these changes became even more pronounced after 2015.

Conversely, people's socioeconomic status (in terms of both wealth and education level) improved over time. From 2000 to 2017, the housing value density increased by 159% and percentage of persons with no high school diploma decreased by 30%, on average. While in the early 2000s more than 50% of the population consisted of non-Hispanic whites, the demographic shift in the study area implies a constant decline of non-Hispanic whites over time. This corresponds with a regional projection that Hispanics would outnumber the white population in Texas in the near future [82, 83].

Corresponding with the decreasing amount of GI, impervious surfaces consistently increased after 2000. Simultaneously, the mean number of dams by county also slightly increased. Yet climatic factors such as mean annual precipitation and flood duration showed unexpected variations by period and were not particularly aligned with the trajectory of flood loss. The highest annual precipitation was reported from 2015 to 2017 (assumably due to the torrential rainfall amounts from Hurricane Harvey in 2017), while flood events with the longest mean duration took place from 2000 to 2002.

3.3. Prediction of flood loss

The results of the pooled OLS, standard fixed effects, and spatially weighted fixed effects models listed in Table 3 display the significant relationship between GI configuration and flood loss. More GI indicators show significant contributions when the spatial autocorrelation of errors in flood loss is controlled for in the model (see the FE SEM results in Table 3). The size, shape complexity, and level of isolation and fragmentation measured by PLAND, SHAPE, PROX, and ENN are all negatively related to flood loss ($p < 0.01$–0.1), while physical connectedness, quantified by GYRATE, shows a positive association ($p < 0.05$). This finding implies that larger, more irregular, more dispersed (or isolated), and less connected configurations of GI patches in a county tend to reduce the financial cost of flood damage over time. More specifically, flood damage decreases by 5.6% for every 0.1 percent-point increase in GI amount of a county. Large, clustered patches with high PROX values also benefit flood mitigation. The computation of standardized coefficients for the OLS model reveals that PROX is the most powerful GI indicator for predicting flood loss ($b^* = -0.45$, $p < 0.1$), followed by SHAPE ($b^* = -0.24$, $p < 0.1$).

When holding other variables constant, the socioeconomic attributes of housing value density and race consistently show significant contributions to flood loss prediction in both the non-spatially and spatially weighted fixed effects models. Decreasing housing value density within a county correlates with a steadily increasing level of flood damage, as expected ($b = -12.35$, $p < 0.01$ in FE SEM). Conversely, an increasing proportion of non-Hispanic whites unexpectedly increases flood losses over time ($b = 0.99$, $p < 0.05$). Within the study area, non-Hispanic whites tend to cluster around floodplain areas, possibly to enjoy more access to water, increasing their vulnerability to flood risks. In the OLS model, climatic factors including annual precipitation and flood duration are found to be the most contributing control variables to flood losses ($b*$ =0.41 and 0.39, respectively). Larger storms with longer durations are found to longitudinally increase flood losses in a county. However, installation of flood control reservoirs and dams helps to moderate this risk (b = -5.00, p < 0.01).

The significant spatial autoregressive parameter (θ) in the spatial panel model confirms the importance of controlling for autocorrelation in flood loss errors (b = 0.24, p < 0.05). The within R-squared statistic shows that the model can account for over 56% of over-time variance in flood damage. The increased log-likelihood and decreased Akaike's and Bayesian Information Criteria (AIC/BIC) also suggest that the spatial panel model (or fixed effects SEM) provides the best model performance. Although the specific effects of time-invariant variables cannot be identified in this model, biased variables in the pooled OLS model imply the importance of county's fixed effects fully controlled for in the other panel data models; the fixed effects SEM in particular corrects the largely underestimated impacts of GI patterns in the OLS model.

Table 3. Pooled OLS, fixed effects, and fixed effects spatial error models predicting logged flood losses per capita.

Variable	β_{OLS} (std)	β_{FE} (std)	$\beta_{FE\ SEM}$ (std)
Spatial patterns of GI			
PLAND	-0.026	-0.744**	-0.546*
	(0.083)	(0.374)	(0.307)
SHAPE	-10.838*	-29.365*	-31.677**
	(6.294)	(17.225)	(14.561)
PROX	-0.00002*	-0.00008	-0.00008*
	(0.00001)	(0.00006)	(0.00004)
ENN	-0.180	-0.467	-0.566***
	(0.167)	(0.284)	(0.177)
COHESION	-2.942	-3.930	-4.869
	(3.674)	(6.578)	(4.380)
GYRATE	0.252	1.159*	0.979**
	(0.246)	(0.648)	(0.381)
Socioeconomic attributes			
Housing value density (logged)	-0.717	-13.567***	-12.351***

	(1.239)	(4.845)	(4.287)
Undereducation	-0.182	0.164	-0.063
	(0.145)	(0.338)	(0.284)
Race	-0.061	1.124**	0.990**
	(0.058)	(0.488)	(0.479)
Built environment			
Impervious area	-0.391	0.228	0.280
	(0.268)	(1.466)	(0.879)
Dams	0.020	-4.627**	-4.989***
	(0.051)	(2.180)	(1.352)
Climatic and geophysical environment			
Precipitation	0.008**	0.007	0.009*
	(0.004)	(0.005)	(0.005)
Duration of flood events	0.790***	0.863***	0.757**
	(0.167)	(0.201)	(0.347)
Surface elevation	12.864		
	(43.959)		
Floodplain area	-0.019		
	(0.074)		
Slope	-1.697		
	(1.769)		
Soil permeability	-0.014		
	(0.107)		
Adjacency to coast	3.638		
	(2.442)		
Distance to coastline	0.087		
	(0.059)		
Time effects			
Period 2	3.618**	15.028***	14.390***
	(1.611)	(3.425)	(2.910)
Period 3	1.480	20.373***	19.230***
	(2.005)	(5.476)	(4.214)
Period 4	3.807	22.987***	21.706***
	(2.314)	(7.035)	(5.613)
Constant	315.496 (361.306)	499.435 (669.736)	
Spatial error (θ)			0.241** (0.115)
Observation (NT)	144	144	144
Log-likelihood	-452.1	-427.4	-424.8
R^2_{within}		0.569	0.563
$R^2_{between}$		0.001	0.001
R^2	0.530	0.002	0.002
AIC	950.243	888.871	885.699
BIC	1,018.548	939.358	939.156

Note. In all specifications, the dependent variable is the logged flood damage cost per capita in 2015 dollars; the value represented in each cell denotes the estimated parameter (β) of a corresponding predictor by model type, and standard errors are exhibited in parenthesis. *$p<0.1$*; *** $p < 0.05$; *** $p < 0.01$.*

4. Discussion

A lack of longitudinal monitoring of GI and its associated effects have impeded the proper restoration and maintenance of regional ecosystem assets crucial for long-term flood protection.

Due to the increasing frequency of natural disasters, the need for GI restoration is increasingly being recognized. However, a gap between planning and implementation still exists [84]. Social and economic constraints such as limited funding initiatives, high implementation costs, and a lack of landowner participation have all hampered successful GI restoration [85]. Similarly, the preservation of GI has often been neglected when development demands are high and alternative engineering techniques such as reservoirs, dams, and drainage pipes provide a false sense of security, allowing residents to believe that the ever-increasing risk of flooding will be offset by these costly structural techniques [10]. However, the results of this study clearly show how the loss of GI over time can bring huge financial burdens to both communities and local governments responsible for reconstructing damaged property. This damage will repeatedly and more intensely occur in the future, exacerbated by climate change and the increasing storm frequency and intensity it entails [86].

According to this research's findings, the strategic planning of GI configurations should be integrated into land use policymaking. Doing so will help minimize economic losses from floods and promote the long-term preservation of natural resources. The results of the spatial panel data modelling completed for this study suggest that adding 0.1% of GI (270 ha on average, that is equivalent to the size of Cornwall Park in Auckland, New Zealand) will help to avoid approximately 5.6% of flood damage in a county (see Table 3). In Harris County, the coverage of impervious surfaces was exceptional (above 30%). This county experienced the greatest expansion of urban area in the sample (5.9% between 2000 and 2017), and the total damage peaked in the most recent period ($20 billion between 2015 and 2017). Restoring, preserving, and increasing the GI amount should be of top priority there, in order to mitigate further flood damage. It can be inferred that the long-term net benefits of investing in regional GI preservation and providing incentives for restoring damaged or lost GI as well as provisions for the addition of new patches are substantial, especially in terms of avoiding repeated financial expenses related to reconstructing damaged housing structures.

In addition to the size of the GI, the findings of this research also suggest that maintaining substantial shape complexity in GI patches is important; in other words, more irregular forms of GI are preferable to standardized, square patterns in terms of effective flood mitigation. This result is consistent with findings from a recent study showing that a coastal flood vulnerability index rating decreased as the shape complexity of urban forests increased [87]. Although there is insufficient scholarly evidence to support the physical basis of this causal relationship, a theoretical reason is conceivable. According to the theory of landscape ecology, flows and exchanges of material and energy occur across boundaries of heterogeneous landscapes [88]. Features of patches determine permeability across their edges [89]. The increased edges of irregularly shaped GI may increase the hydrological interaction between GI and non-GI surfaces, allowing more surface flow to be exchanged, and consequently intercepted and stored by GI. Contrastingly, gridded patterns mainly defined by roads in urbanized areas have standardized GI patterns, threatening their sustainability over time (see Table 2).

Together, the PROX and ENN variables account for the level of isolation and fragmentation of GI. The negative impacts shown in this research of PROX and ENN on local flooding are supported by the findings of recent cross-sectional studies [31, 32]. The longitudinal assessment in this study also revealed the benefits of restoring and maintaining larger patches in closer proximity in order to mitigate flood loss over time. At the same time, GI patches should be better dispersed throughout a county to preserve high in-between distances (ENN). In urban areas in the selected counties, the decreasing distance between GI patches was often associated with fragmentation. Large GI patches were encroached upon and dissected by new developments such as roads and residential houses, decreasing mean ENN values and exacerbating flood damage (see Figure 3). This finding underscores the importance of regulating the ongoing fragmentation of existing GI at the expense of new development. Regional and local governments should internalize increasing flood damage costs in the permitting process for developments near protected GI. Conservation easements for large, clustered GI areas will also be beneficial for maintaining high proximity. Another observation within the study area was that small, interstitial GI patches between large GI areas had largely been destroyed over time. To compensate for this loss, land use policy should guide the restoration and installation of new GI to be large in size, irregularly shaped, and close to previously preserved sites, with multiple clusters placed in a dispersed manner throughout the county to maintain large distances in between GI components.

Finally, the positive relationship between GI connectivity and flood loss found in this study is inconsistent with the findings of previous research; connectivity was often found to lose significance when predicting flood factors [2, 28, 51]. The connected form of GI has been highly valued in landscape ecology, in that connectivity promotes the functional linkage of ecosystems and preserves habitat biodiversity [90]. However, several hydrological studies supported distributed patterns of site-scale flood control systems over centralized and connected patterns in order to capture floodwater from multiple development sources in urban watersheds [91-93]. While the spatial scope of this study was focused beyond that of urban areas, the corresponding results of GYRATE, together with ENN, demonstrate the overweighted importance of dispersed arrangements over connected and clustered forms of GI at the county level. Yet, caution is required with this interpretation. The impacts of changes in connectivity can vary by GI type and geographic location. Within the selected coastal watershed counties, connected forests and woody wetlands were clustered in eastern coastal areas, while shrublands were connected in western coastal areas and scattered in the east. Emergent herbaceous wetlands were generally clustered along the Gulf of Mexico. Since this study limits spatial assessment to a combined class of multiple GI types, further examination is needed to confirm the distinguishing effects of individual GI classes on flood losses.

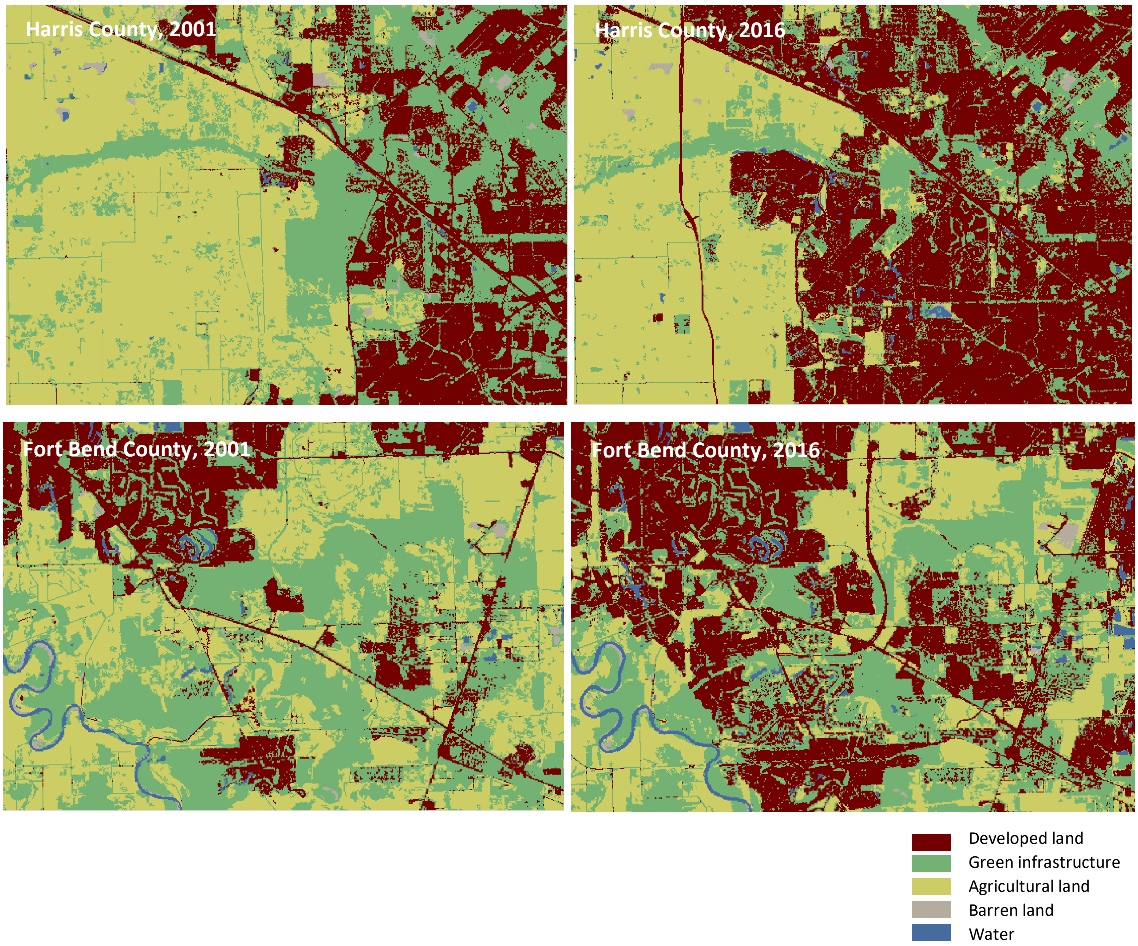

Figure 3. Fragmentation of GI by new developments along the urban periphery: (upper) land cover maps of Harris County in 2001 and 2016 and (lower) land cover maps of Fort Bend County in 2001 and 2016.

5. Conclusion

The longitudinal performance of GI configuration has been underexplored in terms of its ability to reduce flood damage. A few cross-sectional analyses have been conducted, though a limited understanding of spatial autocorrelation would have resulted in statistical bias in the model predictions. This study adopted an advanced method of controlling for spatially correlated errors in flood loss and examined the longitudinal impacts of GI arrangements on flood damage cost at a county level. For the time period between 2000 and 2017, we developed pooled OLS, fixed effects (not spatially weighted), and fixed effects SEMs using a series of GI pattern, socioeconomic status, and built, climatic, and geophysical environment variables. The results reveal that larger, more irregular, more dispersed, less fragmented, and less connected configurations of GI should be restored and preserved over time to minimize the financial cost of flood damage by county. Maintaining larger patches in closer proximity should be top priority, based on the finding that PROX is the strongest GI predictor in the model. To avoid further loss of GI patterning to increasing demands for development in coastal regions, multiple non-structural approaches to protect GI, such as conservation easements, transfers of development rights, land acquisition, buffers/setbacks, incentivization, and zoning should be coupled with the restoration and expansion of existing GI areas.

Although this study provides insightful results, the analysis unit was limited to a regional jurisdiction: the county. A multi-scale analysis would enhance the collective capacity of federal, state, and local governments to achieve a consistent goal of GI protection. Beyond political or geographic boundaries, a watershed-level analysis ought also to be undertaken for integrated flood mitigation. Another limitation of this research is the data merge method from multiple sources. In particular, the national hazard loss database used in this study can be subject to temporal or geographic bias derived by uninsured losses or underestimated minor events [47]. In future research, the time-varying effects of GI patterns should be further analyzed by exploring their interactions with time and developing advanced statistical methods [94]. It should be noted that the panel data method adopted in this study assumed that the longitudinal effects of GI changes were constant over the time periods examined. Moreover, supportive planning measures that protect existing GI and promote strategic placement should also be specified in model prediction to attest their effectiveness. The models would then serve as an important tool for planners and natural resource managers seeking to prioritize possible planning options. Finally, this study's scope was limited to predicting avoidable flood damage costs by maintaining a healthy GI structure over time. Future research should quantify the net economic benefits of restoring and preserving GI by comparing the results with installation, maintenance, and operation costs. Yet, it is important to note that the benefits of GI are not limited to only the economic domain, but rather embrace multifaceted environmental and social values. These holistic, multi-purpose benefits should be appreciated in future studies, despite the low investment returns that GI may sometimes produce, especially in the short term.

References

1. Smith, A.B., *2010–2019: A Landmark Decade of Us. Billion-Dollar Weather and Climate Disasters.* National Oceanic and Atmospheric Administration, 2020.
2. McDonough, K.R., S.L. Hutchinson, J. Liang, T. Hefley, and J.S. Hutchinson, *Spatial Configurations of Land Cover Influence Flood Regulation Ecosystem Services.* Journal of Water Resources Planning and Management, 2020. **146**(11): p. 04020082.
3. Woodruff, J.D., J.L. Irish, and S.J. Camargo, *Coastal Flooding by Tropical Cyclones and Sea-Level Rise.* Nature, 2013. **504**(7478): p. 44-52.
4. Jha, A.K., T.W. Miner, and Z. Stanton-Geddes, *Building Urban Resilience: Principles, Tools, and Practice.* 2013: The World Bank.
5. NOAA. *Billion-Dollar Weather and Climate Disasters: Mapping.* 1980-2020* Billion-Dollar Flooding, Severe Storm, and Tropical Cyclone Disaster Cost (CPI-Adjusted) 2020 [cited 2020 Dec 21]; Available from: https://www.ncdc.noaa.gov/billions/mapping/cost/1980-2020.
6. Sohn, W., S.D. Brody, J.-H. Kim, and M.-H. Li, *How Effective Are Drainage Systems in Mitigating Flood Losses?* Cities, 2020. **107**: p. 102917.
7. Costanza, R., O. Pérez-Maqueo, M.L. Martinez, P. Sutton, S.J. Anderson, and K. Mulder, *The Value of Coastal Wetlands for Hurricane Protection.* A Journal of the Human Environment, 2008. **37**(4): p. 241-248.
8. Brody, S.D., W.G. Peacock, and J. Gunn, *Ecological Indicators of Flood Risk Along the Gulf of Mexico.* Ecological Indicators, 2012. **18**: p. 493-500.
9. USEPA, *Wetlands - Status and Trends.* 2010, United State Environmental Protection Agency.
10. Su, Y.-S., *Discourse, Strategy, and Practice of Urban Resilience against Flooding.* Business and Management Studies, 2016. **2**(1): p. 73-87.
11. Sohn, W., J.-H. Kim, and M.-H. Li, *Low-Impact Development for Impervious Surface Connectivity Mitigation: Assessment of Directly Connected Impervious Areas (Dcias).* Journal of Environmental Planning and Management, 2017. **60**(10): p. 1871-1889.
12. Sohn, W., J.-H. Kim, M.-H. Li, and R. Brown, *The Influence of Climate on the Effectiveness of Low Impact Development: A Systematic Review.* Journal of Environmental Management, 2019. **236**: p. 365-379.
13. Benedict, M.A. and E.T. McMahon, *Green Infrastructure: Smart Conservation for the 21st Century.* Renewable Resources Journal, 2002. **20**(3): p. 12-17.
14. Gill, S.E., J.F. Handley, A.R. Ennos, and S. Pauleit, *Adapting Cities for Climate Change: The Role of the Green Infrastructure.* Built Environment, 2007. **33**(1): p. 115-133.
15. Tzoulas, K., K. Korpela, S. Venn, V. Yli-Pelkonen, A. Kaźmierczak, J. Niemela, and P. James, *Promoting Ecosystem and Human Health in Urban Areas Using Green Infrastructure: A Literature Review.* Landscape and Urban Planning, 2007. **81**(3): p. 167-178.
16. Koc, C.B., P. Osmond, and A. Peters, *Evaluating the Cooling Effects of Green Infrastructure: A Systematic Review of Methods, Indicators and Data Sources.* Solar Energy, 2018. **166**: p. 486-508.
17. Miller, S.M. and F.A. Montalto, *Stakeholder Perceptions of the Ecosystem Services Provided by Green Infrastructure in New York City.* Ecosystem Services, 2019. **37**: p. 100928.
18. Brody, S.D., W.E. Highfield, R. Blessing, T. Makino, and C.C. Shepard, *Evaluating the Effects of Open Space Configurations in Reducing Flood Damage Along the Gulf of Mexico Coast.* Landscape and Urban Planning, 2017. **167**: p. 225-231.
19. Mei, C., J. Liu, H. Wang, Z. Yang, X. Ding, and W. Shao, *Integrated Assessments of Green Infrastructure for Flood Mitigation to Support Robust Decision-Making for Sponge City Construction in an Urbanized Watershed.* Science of the Total Environment, 2018. **639**: p. 1394-1407.
20. Newman, G., W.M. Sohn, and M.-H. Li, *Performance Evaluation of Low Impact Development: Groundwater Infiltration in a Drought Prone Landscape in Conroe, Texas.* Landscape Architecture Frontiers, 2014. **2**(4): p. 122-134.

21. Newman, G.D., A.L. Smith, and S.D. Brody, *Repurposing Vacant Land through Landscape Connectivity.* Landscape Journal, 2017. **36**(1): p. 37-57.
22. Lindell, M.K., R.W. Perry, C. Prater, and W.C. Nicholson, *Fundamentals of Emergency Management*. 2006, FEMA: Washington, DC.
23. Allen, W.L., *Environmental Reviews and Case Studies: Advancing Green Infrastructure at All Scales: From Landscape to Site.* Environmental Practice, 2012. **14**(1): p. 17-25.
24. Liu, W., W. Chen, and C. Peng, *Assessing the Effectiveness of Green Infrastructures on Urban Flooding Reduction: A Community Scale Study.* Ecological Modelling, 2014. **291**: p. 6-14.
25. Ha, G. and J. Jung, *Applying Conservation Easement Policy to River Spaces to Mitigate Natural Hazards in South Korea.* Natural Hazards, 2019. **95**(3): p. 805-822.
26. Brody, S.D. and W.E. Highfield, *Open Space Protection and Flood Mitigation: A National Study.* Land Use Policy, 2013. **32**: p. 89-95.
27. Moccia, F. and A. Sgobbo, *Flood Hazard: Planning Approach to Risk Mitigation and Periphery Rehabilitation.* Management of Natural Disasters, 2016: p. 129-144.
28. Bai, T., A.L. Mayer, W.D. Shuster, and G. Tian, *The Hydrologic Role of Urban Green Space in Mitigating Flooding (Luohe, China).* Sustainability, 2018. **10**(10): p. 3584.
29. Zhang, B., N. Li, and S. Wang, *Effect of Urban Green Space Changes on the Role of Rainwater Runoff Reduction in Beijing, China.* Landscape and Urban Planning, 2015. **140**: p. 8-16.
30. Yuan, Y., G. Fang, M. Yan, C. Sui, Z. Ding, and C. Lu, *Flood-Landscape Ecological Risk Assessment under the Background of Urbanization.* Water, 2019. **11**(7): p. 1418.
31. Li, L., V. Van Eetvelde, X. Cheng, and P. Uyttenhove, *Assessing Stormwater Runoff Reduction Capacity of Existing Green Infrastructure in the City of Ghent.* International Journal of Sustainable Development & World Ecology, 2020: p. 1-13.
32. Kim, H.W. and Y. Park, *Urban Green Infrastructure and Local Flooding: The Impact of Landscape Patterns on Peak Runoff in Four Texas Msas.* Applied Geography, 2016. **77**: p. 72-81.
33. Reja, M.Y., S.D. Brody, W.E. Highfield, and G.D. Newman, *Hurricane Recovery and Ecological Resilience: Measuring the Impacts of Wetland Alteration Post Hurricane Ike on the Upper Tx Coast.* Environmental Management, 2017. **60**(6): p. 1116-1126.
34. Meyer, M.A., M. Hendricks, G.D. Newman, J.H. Masterson, J.T. Cooper, G. Sansom, N. Gharaibeh, J. Horney, P. Berke, and S. van Zandt, *Participatory Action Research: Tools for Disaster Resilience Education.* International Journal of Disaster Resilience in the Built Environment, 2018.
35. Masterson, J., M. Meyer, N. Ghariabeh, M. Hendricks, R.J. Lee, S. Musharrat, G. Newman, G. Sansom, and S. Van Zandt, *Interdisciplinary Citizen Science and Design Projects for Hazard and Disaster Education.* International Journal of Mass Emergencies and Disasters, 2019. **37**(1): p. 6.
36. NOAA, *Defining Coastal Counties*. 2010, National Oceanic and Atmospheric Administration: Washington, DC.
37. Brody, S.D., S. Zahran, W.E. Highfield, H. Grover, and A. Vedlitz, *Identifying the Impact of the Built Environment on Flood Damage in Texas.* Disasters, 2008. **32**(1): p. 1-18.
38. Berke, P.R. and M.M. Conroy, *Are We Planning for Sustainable Development? An Evaluation of 30 Comprehensive Plans.* Journal of the American Planning Association, 2000. **66**(1): p. 21-33.
39. NRCS, *General Soil Map of Texas*, N.R.C. Service, Editor. 2008, Natural Resources Conservation Service: Washington, DC.
40. Galloway, D.L., D.R. Jones, and S.E. Ingebritsen, *Land Subsidence in the United States*. Vol. 1182. 1999: US Geological Survey.
41. Kasmarek, M.C., R.K. Gabrysch, and M.R. Johnson, *Estimated Land-Surface Subsidence in Harris County, Texas, 1915-17 to 2001*. 2009: US Department of the Interior, US Geological Survey (USGS).
42. Moulton, D.W., *Texas Coastal Wetlands: Status and Trends, Mid-1950s to Early 1990s*. 1997: US Department of the Interior, Fish and Wildlife Service, Southwestern Region.

43. Wilson, S.G. and T.R. Fischetti, *Coastline Population Trends in the United States 1960 to 2008.* 2010: US Department of Commerce, Economics and Statistics Administration, US Census Bureau.
44. Climate Central, *Texas and the Surging Sea: A Vulnerability Assessment with Projections for Sea Level Rise and Coastal Flood Risk*. 2014: Princeton, NJ.
45. CEMHS, *The Spatial Hazard Events and Losses Database for the United States, Version 17.0*, ed. A.S. University. 2018, Phoenix, AZ: Center for Emergency Management and Homeland Security, Arizona State University (http://www.sheldus.org).
46. NWS, *Major Events*. 2020, National Weather Service.
47. Gall, M., K.A. Borden, and S.L. Cutter, *When Do Losses Count? Six Fallacies of Natural Hazards Loss Data.* Bulletin of the American Meteorological Society, 2009. **90**(6): p. 799-810.
48. Brody, S.D., S. Zahran, P. Maghelal, H. Grover, and W.E. Highfield, *The Rising Costs of Floods: Examining the Impact of Planning and Development Decisions on Property Damage in Florida.* Journal of the American Planning Association, 2007. **73**(3): p. 330-345.
49. Highfield, W.E. and S.D. Brody, *Price of Permits: Measuring the Economic Impacts of Wetland Development on Flood Damages in Florida.* Natural Hazards Review, 2006. **7**(3): p. 123-130.
50. Yang, L., S. Jin, P. Danielson, C. Homer, L. Gass, S.M. Bender, A. Case, C. Costello, J. Dewitz, and J. Fry, *A New Generation of the United States National Land Cover Database: Requirements, Research Priorities, Design, and Implementation Strategies.* Journal of Photogrammetry and Remote Sensing, 2018. **146**: p. 108-123.
51. Lee, H.K., *A Spatial Assessment of Green Infrastructure and Its Potential Effectiveness on Streamflow*, in *Dept. of Landscape Architecture and Urban Planning*. 2015, Texas A&M University: College Station, TX.
52. McGarigal, K., *Fragstats Help.* University of Massachusetts: Amherst, MA, USA, 2015.
53. Thiagarajan, M., G. Newman, and S.V. Zandt, *The Projected Impact of a Neighborhood-Scaled Green-Infrastructure Retrofit.* Sustainability, 2018. **10**(10): p. 3665.
54. Jevrejeva, S., L. Jackson, A. Grinsted, D. Lincke, and B. Marzeion, *Flood Damage Costs under the Sea Level Rise with Warming of 1.5 C and 2 C.* Environmental Research Letters, 2018. **13**(7): p. 074014.
55. Zahran, S., S.D. Brody, W.G. Peacock, A. Vedlitz, and H. Grover, *Social Vulnerability and the Natural and Built Environment: A Model of Flood Casualties in Texas.* Disasters, 2008. **32**(4): p. 537-560.
56. Burton, C.G., *Social Vulnerability and Hurricane Impact Modeling.* Natural Hazards Review, 2010. **11**(2): p. 58-68.
57. Cutter, S.L., B.J. Boruff, and W.L. Shirley, *Social Vulnerability to Environmental Hazards.* Social Science Quarterly, 2003. **84**(2): p. 242-261.
58. Highfield, W.E., W.G. Peacock, and S. Van Zandt, *Mitigation Planning: Why Hazard Exposure, Structural Vulnerability, and Social Vulnerability Matter.* Journal of Planning Education and Research, 2014. **34**(3): p. 287-300.
59. Do, D.P., L. Wang, and M.R. Elliott, *Investigating the Relationship between Neighborhood Poverty and Mortality Risk: A Marginal Structural Modeling Approach.* Social Science & Medicine, 2013. **91**: p. 58-66.
60. Ludwig, J., G.J. Duncan, L.A. Gennetian, L.F. Katz, R.C. Kessler, J.R. Kling, and L. Sanbonmatsu, *Neighborhood Effects on the Long-Term Well-Being of Low-Income Adults.* Science, 2012. **337**(6101): p. 1505-1510.
61. Bin, O. and C.E. Landry, *Changes in Implicit Flood Risk Premiums: Empirical Evidence from the Housing Market.* Journal of Environmental Economics and management, 2013. **65**(3): p. 361-376.
62. Noh, Y., *Does Converting Abandoned Railways to Greenways Impact Neighboring Housing Prices?* Landscape and urban planning, 2019. **183**: p. 157-166.

63. Sohn, W., J.-H. Kim, M.-H. Li, R.D. Brown, and F.H. Jaber, *How Does Increasing Impervious Surfaces Affect Urban Flooding in Response to Climate Variability?* Ecological Indicators, 2020. **118**: p. 106774.
64. Shuster, W.D., J. Bonta, H. Thurston, E. Warnemuende, and D. Smith, *Impacts of Impervious Surface on Watershed Hydrology: A Review*. Urban Water Journal, 2005. **2**(4): p. 263-275.
65. Sebastian, A., K. Lendering, B. Kothuis, A. Brand, S.N. Jonkman, P. van Gelder, M. Godfroij, B. Kolen, M. Comes, and S. Lhermitte, *Hurricane Harvey Report: A Fact-Finding Effort in the Direct Aftermath of Hurricane Harvey in the Greater Houston Region*. 2017, Delft University of Technology: Delft University of Technology.
66. Brody, S., H. Kim, and J. Gunn, *Examining the Impacts of Development Patterns on Flooding on the Gulf of Mexico Coast.* Urban Studies, 2013. **50**(4): p. 789-806.
67. Liu, Q. and V. Singh, *Effect of Microtopography, Slope Length and Gradient, and Vegetative Cover on Overland Flow through Simulation.* Journal of Hydrologic Engineering, 2004. **9**(5): p. 375-382.
68. Zheng, W., D. Sun, and S. Li, *Mapping Coastal Floods Induced by Hurricane Storm Surge Using Atms Data.* International Journal of Remote Sensing, 2017. **38**(23): p. 6846-6864.
69. Wu, W., K. McInnes, J. O'grady, R. Hoeke, M. Leonard, and S. Westra, *Mapping Dependence between Extreme Rainfall and Storm Surge.* Journal of Geophysical Research: Oceans, 2018. **123**(4): p. 2461-2474.
70. Hsiao, C., *Panel Data Analysis—Advantages and Challenges.* Test, 2007. **16**(1): p. 1-22.
71. Williams, R., *Panel Data: Very Brief Overview*. 2015, Notre Dame, IN: University of Notre Dame.
72. Torres-Reyna, O., *Panel Data Analysis Fixed and Random Effects Using Stata (V. 4.2).* Data & Statistical Services, Priceton University, 2007: p. 1-40.
73. Hausman, J.A., *Specification Tests in Econometrics.* Econometrica, 1978. **46**(6): p. 1251-1271.
74. Wooldridge, J.M., *Introductory Econometrics: A Modern Approach*. 2016, Toronto, Canada: Nelson Education.
75. Anselin, L., J. Le Gallo, and H. Jayet, *Spatial Panel Econometrics*, in *The Econometrics of Panel Data: Fundamentals and Recent Developments in Theory and Practice*, L. Mátyás and P. Sevestre, Editors. 2008, Springer: Verlag, Berlin.
76. Elhorst, J.P., *Panel Data Models Extended to Spatial Error Autocorrelation or a Spatially Lagged Dependent Variable*. 2001: Research School Systems, Organisation and Management.
77. Anselin, L., *Lagrange Multiplier Test Diagnostics for Spatial Dependence and Spatial Heterogeneity.* Geographical Analysis, 1988. **20**(1): p. 1-17.
78. Anselin, L., *Spatial Econometrics: Methods and Models*. Vol. 4. 2013: Springer Science & Business Media.
79. Belotti, F., G. Hughes, and A.P. Mortari, *Spatial Panel-Data Models Using Stata.* The Stata Journal, 2017. **17**(1): p. 139-180.
80. Belotti, F., G. Hughes, and A.P. Mortari, *Xsmle-a Command to Estimate Spatial Panel Models in Stata.* CEIS, University of Rome Tor Vergat School of Economics, University of Edinburg, 2013.
81. Nielsen-Gammon, J.W., *The 2011 Texas Drought.* Texas Water Journal, 2012. **3**(1): p. 59-95.
82. Huerta, J. and B. Cuartas, *Red to Purple? Changing Demographics and Party Change in Texas*. 2020, Paper prepared for the Annual Meeting of the American Political Science Association, Sept. 10-13, 2020.
83. OSD, *Changing Demographics in Texas*, O.o.t.S. Demographer, Editor. 2020, Office of the State Demographer: Corpus Christi, TX.
84. Wu, T., Y.S. Kim, and M.D. Hurteau, *Investing in Natural Capital: Using Economic Incentives to Overcome Barriers to Forest Restoration.* Restoration Ecology, 2011. **19**(4): p. 441-445.
85. Schweizer, D., M. van Kuijk, P. Meli, L. Bernardini, and J. Ghazoul, *Narratives across Scales on Barriers and Strategies for Upscaling Forest Restoration: A Brazilian Case Study.* Forests, 2019. **10**(7): p. 530.

86. Marsooli, R., N. Lin, K. Emanuel, and K. Feng, *Climate Change Exacerbates Hurricane Flood Hazards Along Us Atlantic and Gulf Coasts in Spatially Varying Patterns.* Nature Communications, 2019. **10**(1): p. 1-9.
87. Kim, M., K. Song, and J. Chon, *Key Coastal Landscape Patterns for Reducing Flood Vulnerability.* Science of The Total Environment, 2020: p. 143454.
88. Forman, R., *Land Mosaics: The Ecology of Landscapes and Regions (1995).* The Ecological Design and Planning Reader. IslandPress, Washington, DC, 2014: p. 217-234.
89. Forman, R.T. and P.N. Moore, *Theoretical Foundations for Understanding Boundaries in Landscape Mosaics*, in *Landscape Boundaries*. 1992, Springer. p. 236-258.
90. Ayram, C.A.C., M.E. Mendoza, A. Etter, and D.R.P. Salicrup, *Habitat Connectivity in Biodiversity Conservation: A Review of Recent Studies and Applications.* Progress in Physical Geography, 2016. **40**(1): p. 7-37.
91. Fahy, B. and H. Chang, *Effects of Stormwater Green Infrastructure on Watershed Outflow: Does Spatial Distribution Matter?* International Journal of Geospatial and Environmental Research, 2019. **6**(1): p. 5.
92. Loperfido, J.V., G.B. Noe, S.T. Jarnagin, and D.M. Hogan, *Effects of Distributed and Centralized Stormwater Best Management Practices and Land Cover on Urban Stream Hydrology at the Catchment Scale.* Journal of Hydrology, 2014. **519**: p. 2584-2595.
93. Zellner, M., D. Massey, E. Minor, and M. Gonzalez-Meler, *Exploring the Effects of Green Infrastructure Placement on Neighborhood-Level Flooding Via Spatially Explicit Simulations.* Computers, Environment and Urban Systems, 2016. **59**: p. 116-128.
94. Liang, X., J. Gao, and X. Gong, *Time-Varying Coefficient Spatial Autoregressive Panel Data Model with Fixed Effects.* Available at SSRN 3484289, 2019.